Experimental Physics Laboratory, Kavli Institute for Particle Astrophysics and Cosmology, Department of Physics and SLAC National Accelerator Laboratory, Stanford University, Stanford, CA 94305, USA. [4]Istituto Nazionale di Fisica Nucleare, Sezione di Pisa, I-56127 Pisa, Italy. [5]Laboratoire AIM, CEA-IRFU/CNRS/Université Paris Diderot, Service d'Astrophysique, CEA Saclay, 91191 Gif sur Yvette, France. [6]Istituto Nazionale di Fisica Nucleare, Sezione di Trieste, I-34127 Trieste, Italy. [7]Dipartimento di Fisica, Università di Trieste, I-34127 Trieste, Italy. [8]Istituto Nazionale di Fisica Nucleare, Sezione di Padova, I-35131 Padova, Italy. [9]Dipartimento di Fisica e Astronomia "G. Galilei", Università di Padova, I-35131 Padova, Italy. [10]Istituto Nazionale di Fisica Nucleare, Sezione di Trieste, and Università di Trieste, I-34127 Trieste, Italy. [11]NASA Goddard Space Flight Center, Greenbelt, MD 20771, USA. [12]Laboratoire Univers et Particules de Montpellier, Université Montpellier 2, CNRS/IN2P3, Montpellier, France. [13]Laboratoire Leprince-Ringuet, École polytechnique, CNRS/IN2P3, Palaiseau, France. [14]Consorzio Interuniversitario per la Fisica Spaziale (CIFS), I-10133 Torino, Italy. [15]Istituto Nazionale di Fisica Nucleare, Sezione di Bari, 70126 Bari, Italy. [16]INAF-Istituto di Astrofisica Spaziale e Fisica Cosmica, I-20133 Milano, Italy. [17]Agenzia Spaziale Italiana (ASI) Science Data Center, I-00133 Roma, Italy. [18]Center for Earth Observing and Space Research, College of Science, George Mason University, Fairfax, VA 22030, USA. [19]Space Science Division, Naval Research Laboratory, Washington, DC 20375-5352, USA. [20]Istituto Nazionale di Astrofisica, Osservatorio Astronomico di Roma, I-00040 Monte Porzio Catone (Roma), Italy. [21]Department of Physics, Stockholm University, AlbaNova, SE-106 91 Stockholm, Sweden. [22]The Oskar Klein Centre for Cosmoparticle Physics, AlbaNova, SE-106 91 Stockholm, Sweden. [23]Royal Swedish Academy of Sciences Research Fellow, funded by a grant from the K. A. Wallenberg Foundation. [24]The Royal Swedish Academy of Sciences, Box 50005, SE-104 05 Stockholm, Sweden. [25]Institut Universitaire de France, 75005 Paris, France. [26]INAF Istituto di Radioastronomia, 40129 Bologna, Italy. [27]Dipartimento di Astronomia, Università di Bologna, I-40127 Bologna, Italy. [28]Dipartimento di Fisica, Università di Udine and Istituto Nazionale di Fisica Nucleare, Sezione di Trieste, Gruppo Collegato di Udine, I-33100 Udine. [29]Università di Udine, I-33100 Udine, Italy. [30]Dipartimento di Fisica "M. Merlin" dell'Università e del Politecnico di Bari, I-70126 Bari, Italy. [31]Center for Research and Exploration in Space Science and Technology (CRESST) and NASA Goddard Space Flight Center, Greenbelt, MD 20771, USA. [32]Department of Physics and Department of Astronomy, University of Maryland, College Park, MD 20742, USA. [33]Fermilab, Batavia, IL 60510, USA. [34]Max-Planck-Institut für Radioastronomie, Auf dem Hügel 69, 53121 Bonn, Germany. [35]Department of Physical Sciences, Hiroshima University, Higashi-Hiroshima, Hiroshima 739-8526, Japan. [36]Istituto Nazionale di Fisica Nucleare, Sezione di Perugia, I-06123 Perugia, Italy. [37]Dipartimento di Fisica, Università degli Studi di Perugia, I-06123 Perugia, Italy. [38]NASA Postdoctoral Program Fellow, USA. [39]Institut für Astro- und Teilchenphysik and Institut für Theoretische Physik, Leopold-Franzens-Universität Innsbruck, A-6020 Innsbruck, Austria. [40]Institute for Cosmic-Ray Research, University of Tokyo, 5-1-5 Kashiwanoha, Kashiwa, Chiba, 277-8582, Japan. [41]Department of Physics and Center for Space Sciences and Technology, University of Maryland Baltimore County, Baltimore, MD 21250, USA. [42]School of Physics and Astronomy, University of Southampton, Highfield, Southampton SO17 1BJ, UK. [43]Funded by a Marie Curie IOF, FP7/2007-2013 grant agreement no. 275861. [44]Centre d'Études Nucléaires de Bordeaux Gradignan, IN2P3/CNRS, Université Bordeaux 1, BP120, F-33175 Gradignan Cedex, France. [45]CNRS, IRAP, F-31028 Toulouse cedex 4, France. [46]GAHEC, Université de Toulouse, UPS-OMP, IRAP, Toulouse, France. [47]Science Institute, University of Iceland, IS-107 Reykjavik, Iceland. [48]CSIRO Astronomy and Space Science, Australia Telescope National Facility, Epping NSW 1710, Australia. [49]Department of Astronomy, Stockholm University, SE-106 91 Stockholm, Sweden. [50]Istituto Nazionale di Fisica Nucleare, Sezione di Torino, I-10125 Torino, Italy. [51]Funded by contract ERC-StG-259391 from the European Community. [52]Department of Astronomy, Department of Physics, and Yale Center for Astronomy and Astrophysics, Yale University, New Haven, CT 06520–8120, USA. [53]Department of Physics, Faculty of Science, Mahidol University, Bangkok 10400, Thailand. [54]Hiroshima Astrophysical Science Center, Hiroshima University, Higashi-Hiroshima, Hiroshima 739-8526, Japan. [55]Istituto Nazionale di Fisica Nucleare, Sezione di Roma "Tor Vergata", I-00133 Roma, Italy. [56]Center for Cosmology, Physics and Astronomy Department, University of California, Irvine, CA 92697-2575, USA. [57]Department of Physics and Astronomy, University of Denver, Denver, CO 80208, USA. [58]Max-Planck-Institut für Physik, D-80805 München, Germany. [59]Funded by contract FIRB-2012-RBFR12PM1F from the Italian Ministry of Education, University and Research (MIUR). [60]Department of Physics, University of Johannesburg, P.O. Box 524, Auckland Park 2006, South Africa. [61]Santa Cruz Institute for Particle Physics, Department of Physics and Department of Astronomy and Astrophysics, University of California at Santa Cruz, Santa Cruz, CA 95064, USA. [62]Department of Physics, The University of Hong Kong, Pokfulam Road, Hong Kong, China. [63]National Research Council Research Associate, National Academy of Sciences, Washington, DC 20001, USA.. [64]NYCB Real-Time Computing Inc., Lattingtown, NY 11560-1025, USA. [65]Institute of Space and Astronautical Science, Japan Aerospace Exploration Agency, 3-1-1 Yoshinodai, Chuo-ku, Sagamihara, Kanagawa 252-5210, Japan. [66]Astronomical Observatory, Jagiellonian University, 30-244 Kraków, Poland. [67]Department of Chemistry and Physics, Purdue University Calumet, Hammond, IN 46323-2094, USA. [68]Department of Physics, Graduate School of Science, Kyoto University, Kyoto, Japan. [69]Institut de Ciències de l'Espai (IEEE-CSIC), Campus UAB, 08193 Barcelona, Spain. [70]Institució Catalana de Recerca i Estudis Avançats (ICREA), Barcelona, Spain. [71]3-34-1 Nishi-Ikebukuro, Toshima-ku, Tokyo 171-8501, Japan. [72]Department of Physics, Center for Cosmology and Astro-Particle Physics, The Ohio State University, Columbus, OH 43210, USA. [73]Praxis Inc., Alexandria, VA 22303, USA. [74]Durtal Observatory, 6 Rue des Glycines, F-49430 Durtal, France. [75]Dipartimento di Fisica "Enrico Fermi", Università di Pisa, Pisa I-56127, Italy. [76]Hamburger Sternwarte, Gojenbergsweg 112, 21029, Hamburg, Germany. [77]Ammon, ID 83401, USA. [78]INAF Osservatorio Astronomico di Trieste, Via G. B. Tiepolo 11, 34131 Trieste, Italy. [79]American Astronomical Society, 2000 Florida Ave NW, Washington, DC 20009–1231, USA. [80]School of Earth and Space Exploration, Arizona State University, P.O. Box 871404, Tempe, AZ 85287–1404, USA. [81]67 Rue Jacques Daviel, Rouen 76100, France. ‡Resident at Naval Research Laboratory, Washington, DC 20375, USA.

SUPPLEMENTARY MATERIALS

www.sciencemag.org/content/345/6196/554/suppl/DC1
Materials and Methods
Supplementary Text
Figs. S1 to S6
Tables S1 to S4
References (*31*–*48*)

26 March 2014; accepted 20 June 2014
10.1126/science.1253947

QUANTITATIVE SOCIAL SCIENCE

A network framework of cultural history

Maximilian Schich,[1,2,3]* Chaoming Song,[4] Yong-Yeol Ahn,[5] Alexander Mirsky,[2] Mauro Martino,[3] Albert-László Barabási,[3,6,7] Dirk Helbing[2]

The emergent processes driving cultural history are a product of complex interactions among large numbers of individuals, determined by difficult-to-quantify historical conditions. To characterize these processes, we have reconstructed aggregate intellectual mobility over two millennia through the birth and death locations of more than 150,000 notable individuals. The tools of network and complexity theory were then used to identify characteristic statistical patterns and determine the cultural and historical relevance of deviations. The resulting network of locations provides a macroscopic perspective of cultural history, which helps us to retrace cultural narratives of Europe and North America using large-scale visualization and quantitative dynamical tools and to derive historical trends of cultural centers beyond the scope of specific events or narrow time intervals.

Quantifying historical developments is crucial to understanding a large variety of complex processes from population dynamics to disease spreading, conflicts, and urban evolution. However, in historical research there is an inherent tension (*1*, *2*) between qualitative analyses of individual historical accounts and quantitative approaches aiming to measure and model more general patterns. We believe that these approaches are complementary: We need quantitative methods to identify statistical regularities, as well as qualitative approaches to explain the impact of local deviations from the uncovered general patterns. We have therefore developed a data-driven macroscopic perspective that offers a combination of both approaches.

We collected data from Freebase.com (FB) (*3*), the General Artist Lexicon (AKL) (*4*–*6*), and the Getty Union List of Artist Names (ULAN) (*7*), representing spatiotemporal birth and death information of notable individuals, spanning a time period of more than two millennia. The data sets are included in the supplementary materials (SM), accompanied by an explanation of their nature and data preparation (*8*) (tables S1 and S2). Potential sources of bias are addressed in the SM, including biographical, temporal, and spatial coverage; curated versus crowd-sourced data; increasing numbers of individuals who are still alive; place aggregation; location name changes and spelling variants; and effects of data set language. Most important, compared with contemporary worldwide migration flux (*9*), our data sets focus on birth-to-death migration within and out of Europe and North America (see fig. S1). Notability of individuals, simply defined as the curatorial decision of inclusion in the respective data set, differs slightly between the more

[1]School of Arts and Humanities, The University of Texas at Dallas, Richardson, TX 75080, USA. [2]Chair of Sociology, in particular of Modeling and Simulation (SOMS), Eidgenössische Technische Hochschule (ETH) Zurich, CH-8092 Zurich, Switzerland. [3]Center for Complex Network Research, Department of Physics, Biology and Computer Science, Northeastern University, Boston, MA 02115, USA. [4]Department of Physics, University of Miami Coral Gables, Coral Gables, FL 33146, USA. [5]School for Informatics and Computing, Indiana University Bloomington, Bloomington, IN 47405, USA. [6]Department of Medicine, Harvard Medical School, and Center for Cancer Systems Biology, Dana-Farber Cancer Institute, Boston, MA 02115, USA. [7]Center for Network Science, Central European University, Budapest 1052, Hungary.
*Corresponding author. E-mail: maximilian.schich@utdallas.edu

current, partly crowd-sourced FB and the expert-curated AKL and ULAN.

There was sufficient data density for historical studies: In each data set, the number of notable individuals with birth and death locations provides substantially more data points over time than the commonly used estimates of the world population before the 20th century (Fig. 1A and fig. S2). Even though death locations are underreported (e.g., 153,000 out of 1.1 million in AKL), the data density was sufficient to construct heat maps or Lexis surfaces (*10*), as used in demography, to reveal death age (ir)regularities during more than five centuries, which enables us to highlight the impact of wars and varying longevity (compare Fig. 1B and fig. S3 for details).

We next added a spatial dimension by plotting the number of deaths versus births in each location (Fig. 1C and fig. S4). The plot distinguishes locations where notable people tended to be born (birth sources) from locations where they tended to die (death attractors). Both long-lived and short-lived death locations were observed, with the short-lived locations representing plane crash

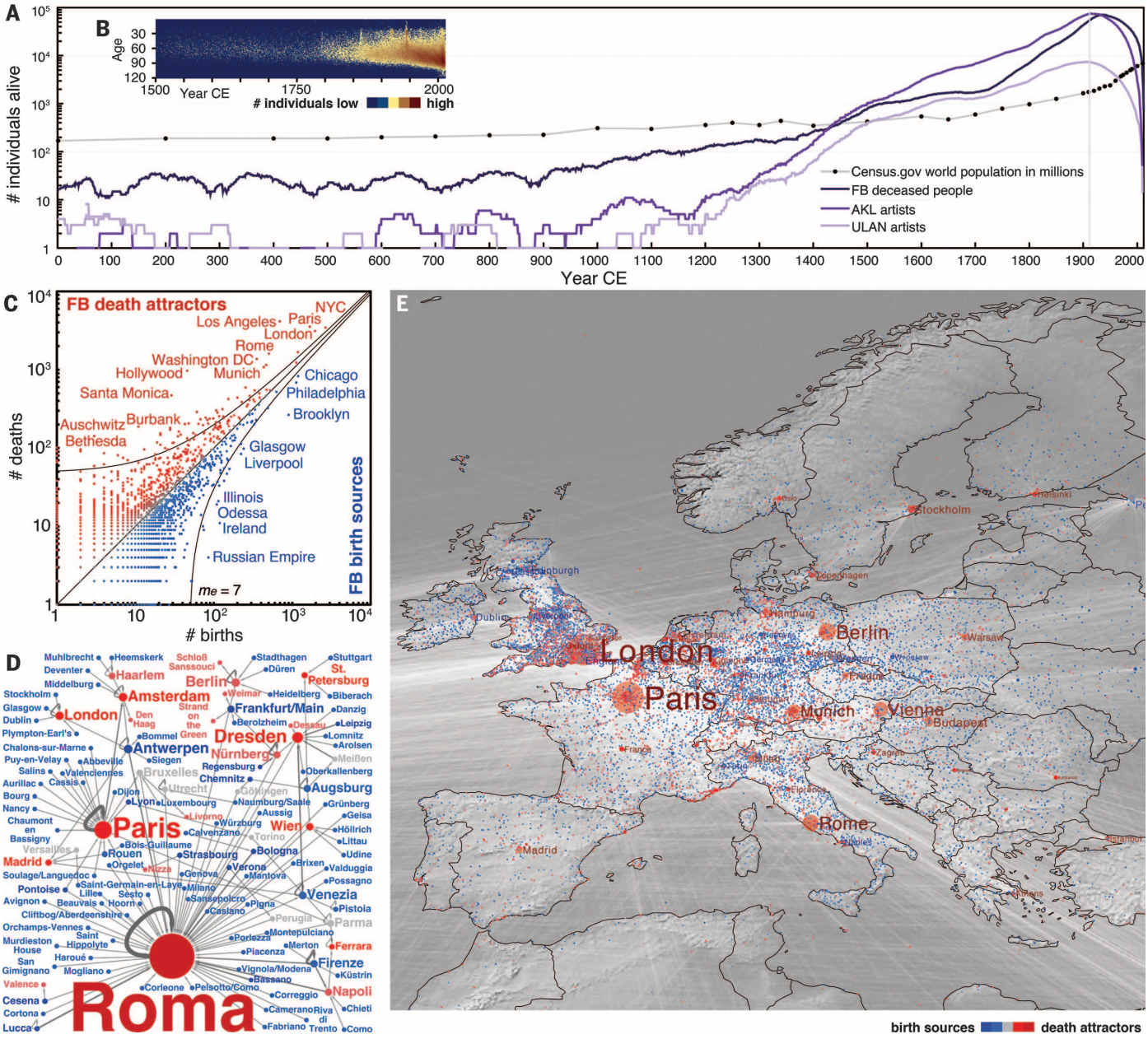

Fig. 1. Birth and death data of notable individuals reveal interactions between culturally relevant locations over two millennia. (**A**) Notable individuals with birth and death locations, alive in a given year from 1 to 2012 CE, for the FB, AKL, and ULAN databases shown together with the estimated world population (in millions, i.e., divided by 10^6 to compare the slope, compare fig. S2). As the data sets grow by orders of magnitude, fluctuations smooth out, allowing for quantification to complement qualitative inquiry. AKL and ULAN grow exponentially with the emancipation of artists around 1200. The decrease after the gray line is due to the fact that we only record individuals with known birth and death dates, and at recent times, more individuals are not yet dead or recorded (details on known biases are in the SM). (**B**) Demographic life table for FB indicating death age frequency from 1500 to 2012 CE (compare fig. S3 for detail). (**C**) Birth-death scatter plot for locations in FB, cumulated over all time with outliers colored as birth sources (blue) and death attractors (red) (see figs. S4 and S13 for dynamics, significance, and further data sets). (**D**) Illustration of birth-death flows of antiquarians in the 18th century, based on the Winckelmann Corpus (*11*), using the color scheme of the scatter plot above. (**E**) Migration in Europe based on FB, with node size corresponding to PageRank (compare figs. S5 to S7 for detail, further regions, and data sets).

sites, battlefields, or concentration camps. We found outliers, where the imbalance of births and deaths results in significant deviations from the diagonal (as defined in the SM under Birth-Death Imbalance). Indeed, highly significant outliers, like Hollywood, had more than 10 times as many deaths as births.

When individual birth and death locations are connected, the resulting network reveals a consistent pattern of cultural attraction and interaction in space. For example, several hundred antiquarians in the 18th century (with data derived from the Winckelmann Corpus) (*11*), died in a number of relevant cultural centers such as Rome, Paris, or Dresden, even though they had been born all over Europe (Fig. 1D; see SM).

We also constructed a worldwide historical migration network, connecting 37,062 locations via the birth-death data of 120,211 individuals in the FB data set from King David in 1069 BCE to Poppy Barlow in 2012 CE (see fig. S5). On a map of Europe (Fig. 1E), the distribution of colors reveals a differentiated landscape of sources (blue, more births) and attractors (red, more deaths). The sizes of nodes represent their importance, estimated by their PageRank, calculated from the underlying migration network (*12*). We chose PageRank, one of the most popular centrality measures, as it offers clear advantages over other centrality measures (compare SM under PageRank versus Eigenvector Centrality), as well as a simple analogy, where every death counts as a vote for the target location, in the same way that hyperlinks are considered as a vote for their target Web site. We find that the PageRank hierarchy intuitively reflects the hierarchy of urban population size (*13*). Yet, although PageRank correlated reasonably well with the number of births in locations ($r = 0.74$), and even better with the number of deaths ($r = 0.97$), it did not predict the imbalance of births and deaths ($r = 0.34$): Large attractive locations, such as London, Paris, or Rome were complemented by many small attractors, e.g., at the French Riviera or both sides of the Alps. Other highly ranked locations, such as Edinburgh or Dublin, were more fertile than deadly, as was most of rural Europe. Additional regions and data sets with similar conclusions are presented in figs. S5 to S7.

The numbers of notable individuals $N(t)$ and locations $S(t)$ grew exponentially over time (Fig. 2A and fig. S8). Yet, the difference in growth rates for individuals (r) and locations (s) implies an underlying Heaps' law (*14*) $S(t) \approx N(t)^{\alpha}$, where $\alpha = s/r \approx 0.9$. The sublinear exponent $\alpha < 1$ indicates that, in the long run, the growth of already existing attractive locations for notable individuals dominates over the emergence of new attractive locations.

The probability distributions of birth locations f_B and death locations f_D, or birth-to-death paths $f_{B \to D}$, follow Zipf's law (Fig. 2B and figs. S9 and S10) (*15*). The nature of the frequency distributions was highly consistent over several centuries, whereas the slopes for birth and death changed gradually over time (Fig. 2B and fig. S10, G to I). To our surprise, the slopes for births and deaths started to differ significantly from the 19th century onward in FB and even earlier for artists in AKL. The difference indicates that larger cultural centers attract a greater proportion of notable individuals, in line with recently discovered urban scaling laws (*16*, *17*). We used an established method to fit a power law to the data to obtain the scaling exponents (*18*). We further confirmed the significant difference between f_B and f_D, using a two-sample Kolmogorov-Smirnov (KS) test comparing birth and death distributions directly (see. fig. S10J).

The distribution of birth-to-death distances Δr changed very little during more than eight centuries (Fig. 2C and fig. S11). The median distance from birth to death has not even doubled between the 14th and the 21st centuries (214 km and 382 km, respectively), with a minimum of 135 km in the 17th century (see vertical lines in Fig. 2C). Only long-range mobility, captured by the tail of the probability distribution $P(\Delta r)$, changed because of the gradual colonization of the world and increasing traffic between the U.S. coasts. As such, these results are consistent with Ravenstein's laws of migration (*19*, *20*), formulated in the late 19th century, and other empirical observations of human mobility in geography, demography, and sociology, from Zipf's intercity movement of persons (*21*) to modern census statistics (*22*) and measurements based on tracking dollar bills or mobile phones (*23*, *24*). Our findings are nevertheless relevant, as (i) we can determine these patterns from a relatively small fraction of birth and death location pairs, and (ii) we demonstrate that the patterns hold for more than eight centuries on an international scale that is not divided by country boundaries.

Aside from these global patterns, we find considerable instabilities on a local level over the order of centuries. The death share, or the relative fraction of notable deaths in specific locations, was highly unstable over centuries (Fig. 2D and fig. S12). This local instability confirms recent expectations regarding the rise and fall of populations in top-ranked cities (*13*, *16*, *25*) but also points to substantial amounts of noise in the system (*26*).

Adding another aspect of local instability, the dynamics of birth-death imbalance for

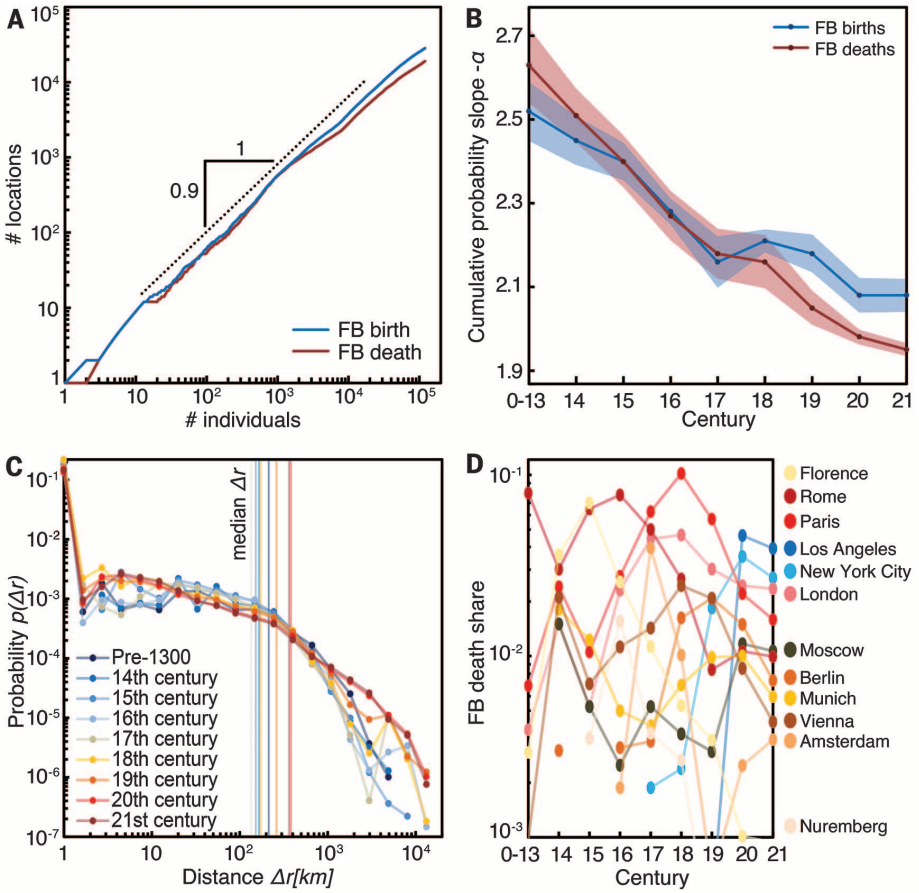

Fig. 2. Birth-death networks provide historical evidence for global patterns and local instabilities in human mobility dynamics. (**A**) The number $N(t)$ of individuals as a function of the number $S(t)$ of locations, where $\alpha = 0.9$ (compare fig. S8 for other data sets). (**B**) Cumulative probability distribution slopes for birth and death frequency in FB locations from before 1300 to 2012 CE. The shaded area indicates the uncertainty of the slope (*18*) (see fig. S10, G to J, for detail and other data sets). (**C**) The fat-tailed distribution of birth-to-death distances Δr in FB exhibits little change over time from before 1300 to 2012 CE (compare fig. S11). (**D**) The relative death share and, consequently, rank of major FB locations over centuries from before 1300 to 2012 CE (compare fig. S12).

individual locations over centuries are tracked in fig. S13, measured as multiples m_e of the square-root-deviation e from the perfectly balanced diagonal in Fig. 1C and fig. S4. In fact, individual locations fluctuate substantially in this respect, as in the case of New York City, which is now a clear death attractor but gave birth to more notable individuals than it attracted around 1920.

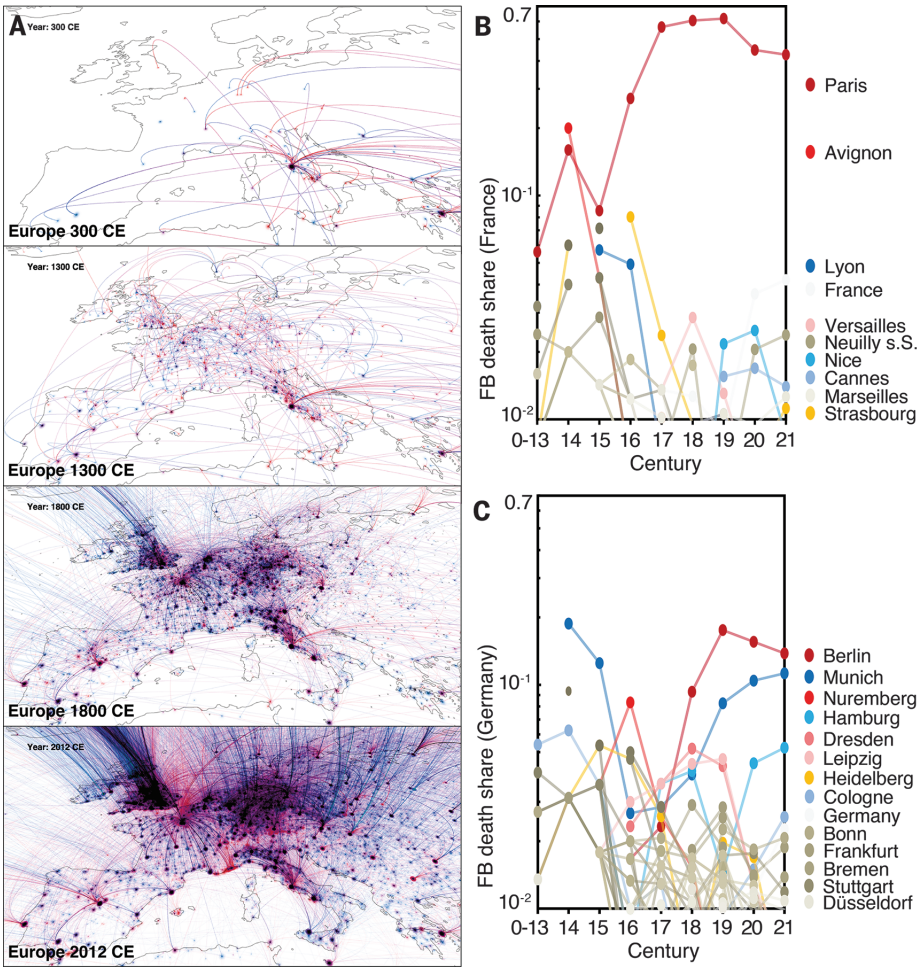

Fig. 3. The visualization of birth-death network dynamics offers a meta-narrative of cultural history. (**A**) A sequence of frames, based on movie S1, exemplifies the FB narrative for Europe from Roman times to the present. The dynamically applied color scheme (with black and white inverted in print) denotes birth-death imbalance (blue to red) (compare Fig. 1C). In the supplementary movie, individuals appear as particles, indicating collective directions of flow as they move toward their death locations. Throughout the movie, local cohesive dynamics emerge regionally in addition to the massive long-range interactions, first from and to Rome and eventually to emergent country capitals and economic centers, including those in the East. The final network state for locations in 2012—within what is now France and Germany—is the result of massive centralization toward Paris versus multicentric competition in Germany. (**B** and **C**) Death-share plots for locations from before 1300 to 2012 CE confirm that France is characterized by a winner-takes-all regime, where Paris takes in a substantial and almost constant share of notable individuals (*27*). Germany, in contrast, is characterized by a subcritical fit-gets-richer regime, where no center surpasses 19% in any given century.

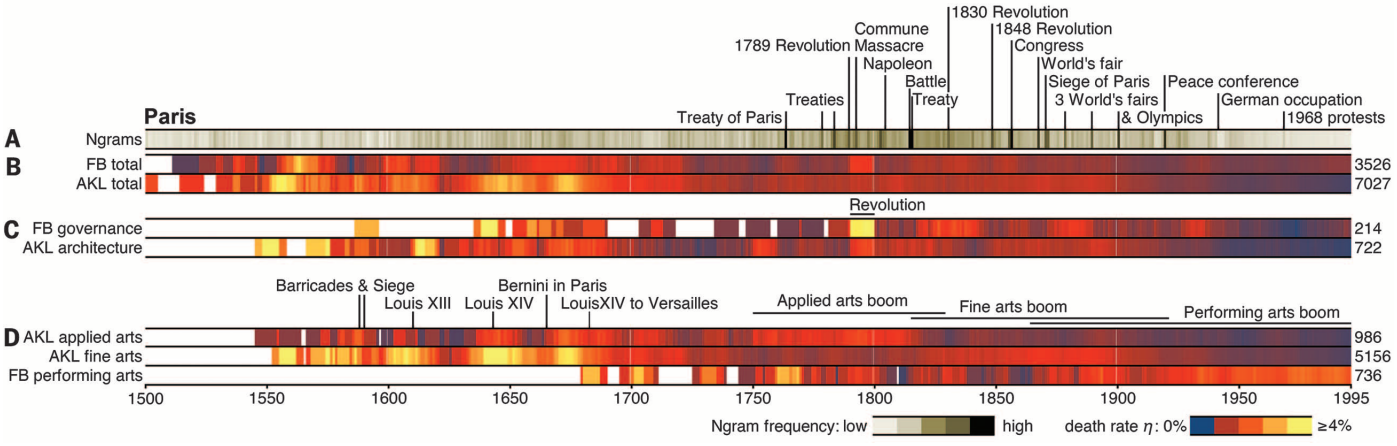

Fig. 4. Temporal death rate patterns in cultural centers reveal midterm trends that are hard to extract from other sources. (**A**) English Google Ngram trajectory for the pattern "Paris in {year}" from 1500 to 1995 CE. Dark spikes point to outstanding historical events in the city, labeled semi-automatically using Web searches, such as "Paris in 1763" returning "Treaty of Paris." (**B**) Paris death rate trajectories for FB total and AKL total indicate deviations from the nearly constant fitness $\eta_i^D(t)$ (compare fig. S16 and our model in the SM). Color indicates periods of accelerated (bright) versus slower growth (dark). The numbers at the ends of the trajectories indicate the respective number of individuals. (**C**) Trajectories for FB governance and AKL architecture positively correlate around the French Revolution from 1785 to 1805 (r = 0.89), whereas FB governance and artists in AKL fine arts slightly negatively correlate (r = −0.34). (**D**) Trajectories for AKL applied arts, AKL fine arts, and FB performing arts.

Next, we illustrate the qualitative relevance of our macroscopic perspective by delineating the meta-narratives of European and North American cultural history, based on birth-death data without additional source material (movies S1 and S2, Fig. 3A, and fig. S14). The sequence of images in Fig. 3A exemplifies the cultural narrative of Europe from 0 to 2012 CE, as presented in movie S1 based on FB: In the beginning, a pan-European elite defined Rome as the center of its empire via massive long-range interactions, followed by increasing point-to-point migration throughout Europe, where Rome remained a hub along with rising subcenters, such as Cordova and Paris. Starting in the 16th century, data density in Europe becomes sufficient to reveal regional clusters. In fact, it becomes evident that Europe is characterized by two radically different cultural regimes: A winner-takes-all regime, with massive centralization toward centers such as Paris, and a fit-gets-richer regime, where many subcenters compete with each other in federal clusters throughout Central Europe and Northern Italy (*27*) (see Fig. 3, B and C, and fig. S15).

After demonstrating the global quantitative and qualitative relevance of our macroscopic approach, we now focus on the dynamics of individual cultural centers, defined as locations with substantial amounts of notable deaths. We examined notable events identified from the Google Ngram English data set (*28*), a procedure that can and should be complemented with data sets in other languages to allow for comparison and eventually worldwide coverage (known biases are discussed in the SM). Recording the frequency of words and word combinations in an estimated 5% of all books ever published, the Google Ngram data were originally used to plot the pattern frequency against book publication dates (*29*). Here, instead, we obtained events by searching for the pattern "{location} in {year}," which allows us to map the "expression" of cultural centers over longer time periods, similar to a gene expression plot (*30*) (Fig. 4A). Particularly after 1750, dark spikes in the trajectory reveal outstanding historical events. Web searches even allow us to semiautomatically add event labels to these spikes. The resulting Ngram trajectories can be examined relative to total death rate trajectories (Fig. 4B and fig. S16), tracking deviations of locations from their nearly constant fitness $\eta_i^D(t)$ (compare fig. S17 and our model in the SM), and even relative to births and deaths within professional genres in FB, AKL, and ULAN (Fig. 4, C and D). By revealing such correlated changes and continuities, our approach allows for cross-fertilization of domain knowledge into other domains, periods, and geographic areas.

REFERENCES AND NOTES

1. R. L. Carneiro, *The Muse of History and the Science of Culture* (Springer, New York, 2000).
2. L. Spinney, *Nature* **488**, 24–26 (2012).
3. Freebase.com: A community-curated database of well-known people, places, and things (Google, Mountain View, CA, 2011); www.freebase.com.
4. A. Beyer, S. Bénédicte, W. Tegethoff, Eds., *Allgemeines Künstlerlexikon (AKL). Die Bildenden Künstler aller Zeiten und Völker* (De Gruyter, Berlin, 1991, rev. ed. 2010).
5. U. Thieme, F. Becker, Eds., *Allgemeines Lexikon der bildenden Künstler von der Antike bis zur Gegenwart* (Seemann, Leipzig, 1907, rev. ed. 1950).
6. H. Vollmer, Ed., *Allgemeines Lexikon der bildenden Künstler des XX. Jahrhunderts* (Seemann, Leipzig, 1953, rev. eds. 1962 and 1980).
7. Getty Vocabulary Program, *Union List of Artist Names* (The J. Paul Getty Trust, Los Angeles, 2010); www.getty.edu/research/tools/vocabularies/ulan/.
8. Materials and methods are available as supplementary materials on *Science* Online.
9. G. J. Abel, N. Sander, *Science* **343**, 1520–1522 (2014).
10. N. Keiding, *Philos. Trans. R. Soc.* **332**, 487–509 (1990).
11. Winckelmann-Gesellschaft Stendal, Eds., Corpus der antiken Denkmäler, die J.J. Winckelmann und seine Zeit kannten [database] (Biering & Brinkmann, München, 2000).
12. S. Brin, L. Page, *Comput. Netw. ISDN Syst.* **30**, 107–117 (1998).
13. M. Batty, *Nature* **444**, 592–596 (2006).
14. H. S. Heaps, *Information Retrieval: Computational and Theoretical Aspects* (Academic Press, Waltham, MA, 1978).
15. G. K. Zipf, *Human Behavior and the Principle of Least Effort: An Introduction to Human Ecology* (Addison-Wesley, Boston, 1949).
16. L. M. A. Bettencourt, J. Lobo, D. Helbing, C. Kühnert, G. B. West, *Proc. Natl. Acad. Sci. U.S.A.* **104**, 7301–7306 (2007).
17. L. M. A. Bettencourt, J. Lobo, D. Strumsky, G. B. West, *PLOS ONE* **5**, e13541 (2010).
18. A. Clauset, C. R. Shalizi, M. E. J. Newman, *SIAM Rev.* **51**, 661–703 (2009).
19. E. G. Ravenstein, *J. Stat. Soc. Lond.* **48**, 167–235 (1885).
20. E. G. Ravenstein, *J. R. Stat. Soc.* **52**, 241–305 (1889).
21. G. K. Zipf, *Am. Sociol. Rev.* **11**, 677–686 (1946).
22. P. Ren, *Lifetime Mobility in the United States: 2010* (U.S. Census Bureau, U.S. Department of Commerce, Washington, DC, 2011).
23. D. Brockmann, L. Hufnagel, T. Geisel, *Nature* **439**, 462–465 (2006).
24. C. Song, T. Koren, P. Wang, A.-L. Barabási, *Nat. Phys.* **6**, 818–823 (2010).
25. D. R. White, T. Laurent, N. Kejzar, in *Globalization as Evolutionary Process: Modeling Global Change*, G. Modelski, T. Devezas, W. R. Thompson, Eds. (Routledge, Milton Park, UK, 2007), pp. 190–225.
26. N. Blumm *et al.*, *Phys. Rev. Lett.* **109**, 128701 (2012).
27. G. Bianconi, A.-L. Barabási, *Phys. Rev. Lett.* **86**, 5632–5635 (2001).
28. Google Ngram English data set, version 20090715 (Google, Mountain View, 2009); http://storage.googleapis.com/books/ngrams/books/datasetsv2.html.
29. J.-B. Michel *et al.*, *Science* **331**, 176–182 (2011).
30. M. J. Hawrylycz *et al.*, *Nature* **489**, 391–399 (2012).

ACKNOWLEDGMENTS

We are grateful to Verlag Walther De Gruyter (AKL), The Getty Research Institute (ULAN), and Biering and Brinkmann (WCEN) for making data available to us and for allowing all data needed to replicate the conclusions of the paper to be available as SM. We furthermore thank our collaborators at BarabásiLab and ETH SOMS for discussions and comments on the manuscript. The work of M.S. was partially supported by German Research Foundation (DFG) grant (no. SCHI 1065/2-1) and The University of Texas at Dallas Arts and Technology (ATEC) Fellowship no. 1. D.H. is grateful for partial support by the European Research Council Advanced Investigator Grant "Momentum" (grant no. 324247).

SUPPLEMENTARY MATERIALS

www.sciencemag.org/content/345/6196/558/suppl/DC1
Materials and Methods
Figs. S1 to S17
Tables S1 and S2
References (*31–61*)
Movies S1 and S2
External Databases S1 to S4

6 May 2013; accepted 13 June 2014
10.1126/science.1240064

DINOSAUR EVOLUTION

Sustained miniaturization and anatomical innovation in the dinosaurian ancestors of birds

Michael S. Y. Lee,[1,2]* Andrea Cau,[3,4] Darren Naish,[5] Gareth J. Dyke[5,6]

Recent discoveries have highlighted the dramatic evolutionary transformation of massive, ground-dwelling theropod dinosaurs into light, volant birds. Here, we apply Bayesian approaches (originally developed for inferring geographic spread and rates of molecular evolution in viruses) in a different context: to infer size changes and rates of anatomical innovation (across up to 1549 skeletal characters) in fossils. These approaches identify two drivers underlying the dinosaur-bird transition. The theropod lineage directly ancestral to birds undergoes sustained miniaturization across 50 million years and at least 12 consecutive branches (internodes) and evolves skeletal adaptations four times faster than other dinosaurs. The distinct, prolonged phase of miniaturization along the bird stem would have facilitated the evolution of many novelties associated with small body size, such as reorientation of body mass, increased aerial ability, and paedomorphic skulls with reduced snouts but enlarged eyes and brains.

The evolution of birds from bipedal carnivorous dinosaurs is one of the most compelling examples of macroevolution (*1–7*). Numerous studies (*1–18*) have documented the cumulative evolution of avian characteristics along the ~160 million year (My) lineage leading from large Triassic theropods (oldest widely accepted records, *Herrerasaurus* and *Eodromaeus*, ~230 million years old) to modern birds (Neornithes; oldest widely accepted record, *Vegavis*, ~67 million years old). Nevertheless, there remain many intriguing questions regarding size and anatomical evolution along the bird stem lineage. Theropods were typically large to gigantic, but small body size characterized all taxa near the origin of forewing-powered flight in birds [Avialae *sensu* (*1–3*), Aves *sensu* (*15*)]. It has been both proposed (*4–8*) and contested (*9–11*) that sustained trends of size reduction occurred within theropod evolution. However, most